Apoptosis Imaging Probe Predicts Early Chemotherapy Response in Preclinical Models: A Comparative Study with ^{18}F-FDG PET

Shaoli Song[1,2], Chiyi Xiong[2], Wei Lu[2,3], Geng Ku[2], Gang Huang[1], and Chun Li[2]

[1]*Department of Nuclear Medicine, Renji Hospital, Shanghai Jiaotong University, School of Medicine, Shanghai, China;* [2]*Department of Experimental Diagnostic Imaging, University of Texas MD Anderson Cancer Center, Houston, Texas; and* [3]*Department of Biomedical and Pharmaceutical Sciences, College of Pharmacy, University of Rhode Island, Kingston, Rhode Island*

Previously, we reported a small-molecular-weight peptide, single amino acid chelae(^{99m}Tc)-conjugated phosphatidylserine-binding peptide (SAAC(^{99m}Tc)-PSBP-6), with high binding affinity to phosphatidylserine on the surface of apoptotic cells. The purpose of this study was to determine the effectiveness of SAAC (^{99m}Tc)-PSBP-6 in detecting apoptosis induced by chemotherapy. **Methods:** B16/F10 melanoma and 38C13 lymphoma tumor models were used in this study. For each type of tumor model, mice were divided into a group treated for imaging (treated group [TG]) and a control group that was not treated (nontreated group [N-TG]). In the TG, mice bearing murine B16/F10 melanoma received a single dose of intravenous polymeric paclitaxel (equivalent dose, 80 mg/kg), and mice bearing 38C13 xenografts received intraperitoneal cyclophosphamide (100 mg/kg). Mice in the N-TG were given the same volume of saline. γ-imaging 4 h after intravenous injection of SAAC(^{99m}Tc)-PSBP-6 and small-animal PET 1 h after intravenous injection of ^{18}F-FDG were performed before chemotherapy and at 1 d after chemotherapy. On day 1, immediately after the apoptosis imaging sessions, 3 mice each in the TGs and N-TGs were killed, and tumor tissues were excised for hematoxylin and eosin histology, autoradiography, and immunohistochemical staining using anti–active caspase 3 and terminal deoxynucleotidyl transferase-mediated dUTP nick-end labeling (TUNEL). The tumor volumes in the remaining mice (n = 5/group) were measured every other day for 7 d. **Results:** In both tumor models, the uptake of SAAC (^{99m}Tc)-PSBP-6 increased significantly on day 1 after treatment, whereas ^{18}F-FDG uptake decreased significantly during the same time. The mean tumor uptake values for SAAC(^{99m}Tc)-PSBP-6 increased 142.4% ± 36.9% and 112% ± 42.9% in 38C13 and B16/F10 tumors, respectively (both $P < 0.05$, pretreatment vs. day 1 after treatment). The mean tumor uptake value for ^{18}F-FDG decreased 67.36% ± 17.52% and 62.82% ± 4.53% in 38C13 and B16/F10 tumors, respectively. The uptake of SAAC (^{99m}Tc)-PSBP-6 negatively correlated with ^{18}F-FDG (r = –0.79, $P < 0.05$). Treated tumors had smaller volumes than untreated controls, treated tumors had significantly higher numbers of apoptotic cells, and tumor uptake of SAAC(^{99m}Tc)-PSBP-6 correlated with the number of TUNEL-positive cells. **Conclusion:** SAAC (^{99m}Tc)-PSBP-6 γ-imaging is useful for the early assessment of treatment-induced apoptosis and, thus, may be used as a substitute for ^{18}F-FDG PET for assessing early treatment response.

Key Words: SAAC(^{99m}Tc)-PSBP-6; apoptosis imaging; ^{18}F-FDG; PET; chemotherapy

J Nucl Med 2013; 54:104–110
DOI: 10.2967/jnumed.112.109397

Chemotherapy is one of the most widely used treatments for cancer of all types. Unfortunately, chemotherapy is effective in only a subset of patients. Accurate early assessment of response to chemotherapy may prevent unnecessary toxicity and costs associated with ineffective treatment and enable the tailoring of treatment regimens to individual patients.

Noninvasive imaging with ^{18}F-FDG PET enables the monitoring of changes in metabolic activity and has become a gold standard for the assessment of early treatment response (*1–4*). ^{18}F-FDG is a glucose analog that reflects glucose metabolic activity in tumor cells; an effective therapy often leads to a significant decrease in ^{18}F-FDG uptake. However, ^{18}F-FDG is not a tumor-specific agent. Inflammatory cells, which infiltrate tumors as a result of chemotherapy, also have a high intracellular accumulation of ^{18}F-FDG, perhaps even higher than that of the viable tumor cells, leading to an underestimation of the therapeutic effect (*5–7*). Moreover, some molecularly targeted drugs are cytostatic—that is, they seem not to alter glucose metabolism enough for ^{18}F-FDG PET to have significant predictive value (*8*). Therefore, the development of an imaging technique that is capable of more accurately predicting early treatment response would benefit cancer patients undergoing anticancer molecular therapy and chemotherapy.

Apoptosis plays an important role in both normal physiology and many disease processes (*9–11*). Because

Received May 26, 2012; revision accepted Sep. 4, 2012.
For correspondence or reprints contact either of the following:
Shaoli Song, Department of Nuclear Medicine, RenJi Hospital, Shanghai Jiaotong University, School of Medicine, Shanghai, China, 200127.
E-mail: shaoli-song@163.com
Chun Li, Department of Experimental Diagnostic Imaging–Unit 59, University of Texas MD Anderson Cancer Center, 1515 Holcombe Blvd., Houston, TX 77030.
E-mail: cli@mdanderson.org

successful treatments induce cancer cell apoptosis soon after the treatments are initiated (*12,13*), accurate imaging of apoptosis may permit the noninvasive assessment of disease states and early response to therapeutic interventions (*14*). Although several apoptosis-avid imaging agents, including radiolabeled annexin V (*15–18*), synaptotagmin (*19,20*), and caspase inhibitors (*21,22*), have been explored as potential probes for imaging apoptosis, to date, no PET or SPECT/CT tracer for imaging apoptosis is available for clinical use (*23,24*).

In our previous work, we identified a 14-mer peptide SAAC(M)FNFRLKAGQKIRFG (SAAC(Re)-PSBP-6 and SAAC(^{99m}Tc)-PSBP-6) that showed a nanomolar binding affinity (26 nM) to phosphatidylserine), a phospholipid exposed on the outer leaflet of the apoptotic cell membrane (*25*). The purpose of this study was to confirm the potential clinical utility of SAAC(^{99m}Tc)-PSBP-6 for assessing early treatment response to chemotherapy by comparing SAAC (^{99m}Tc)-PSBP-6 as an apoptosis γ-imaging agent with ^{18}F-FDG as a metabolism small-animal PET agent in 38C13 lymphoma and B16/F10 melanoma tumor models.

MATERIALS AND METHODS

Radiopharmaceuticals

Poly(L-glutamic acid)-paclitaxel (PG-TXL) was synthesized as previously reported (*26*). The polymeric drug conjugate was dissolved in saline before injection. Cyclophosphamide monohydrate was purchased from MP Biomedicals. SAAC(^{99m}Tc)-PSBP-6 was synthesized according to our previously reported procedures (*25*). The structure of SAAC(^{99m}Tc)-PSBP-6 is shown in Supplemental Figure 1 (supplemental materials are available online only at http://jnm.snmjournals.org). The radiolabeling efficiency and specific activity of SAAC(^{99m}Tc)-PSBP-6 were greater than 95% and 7.4 MBq (0.2 mCi)/μg, respectively. ^{18}F-FDG was obtained from the Department of Nuclear Medicine at the University of Texas MD Anderson Cancer Center.

Cell Lines

Murine B-cell lymphoma 38C13 cells were a gift from Professor Tove Olafsen (University of California at Los Angeles). The cells were maintained in RPMI 1640 medium supplemented with 10% heat-inactivated fetal bovine serum, 2 mM L-glutamine, penicillin at 100 U/mL, streptomycin at 100 mg/mL, and 50 mM 2-mercaptoethanol. All medium and supplements were obtained from Invitrogen. The B16/F10 cell line was obtained from the American Type Culture Collection. The cells were maintained in Dulbecco modified Eagle medium and F-12 medium supplemented with 10% fetal bovine serum and 1% penicillin–streptomycin and were incubated at 37°C with 5% CO_2 and 100% humidity.

Animal Models

Nu/Nu nude mice and C3H/HeJ mice (age, 4–6 wk) were purchased from Charles River Laboratories. The mice were kept under specific pathogen-free conditions and were handled and maintained according to guidelines of the Institutional Animal Care and Use Committee. The 38C13 cells (1×10^7 cells/100 μL) were inoculated subcutaneously into the right shoulders of 6- to 8-wk-old female C3H/HeJ mice. B16/F10 cells (1×10^6 cells/100 μL) were inoculated subcutaneously into the right shoulders of Nu/ν-mice. When the tumors had grown to 8–10 mm in diameter, the mice were used in the following experiments.

Study Design

Figure 1 summarizes the study design comparing γ-imaging using SAAC(^{99m}Tc)-PSBP-6 with small-animal PET using ^{18}F-FDG in tumor-bearing mice after chemotherapy. Sixteen 38C13 tumor–bearing mice and 16 B16/F10 tumor–bearing mice were used in the experiments. For each tumor model, mice were randomly divided into treated groups (TGs, $n = 8$) and nontreated groups (N-TGs, $n = 8$). Mice in the TGs underwent γ-imaging with SAAC(^{99m}Tc)-PSBP-6, followed by ^{18}F-FDG small-animal PET before chemotherapy. The time interval between γ-imaging and small-animal PET imaging was 6 h. Then, the mice bearing 38C13 tumors received an intraperitoneal injection of cyclophosphamide at a dose of 100 mg/kg, and the mice bearing B16/F10 tumors received an intravenous injection of PG-TXL at an equivalent paclitaxel dose of 80 mg/kg. Imaging studies were performed again at 24 h after treatment (day 1). γ-imaging was performed on all 8 mice in each treatment group at 4 h after intravenous injection of SAAC(^{99m}Tc)-PSBP-6 (7.4 MBq [200 μCi]/mouse). Three of the 8 treated mice in each treatment group were killed, and the tumors were collected for autoradiography, hematoxylin

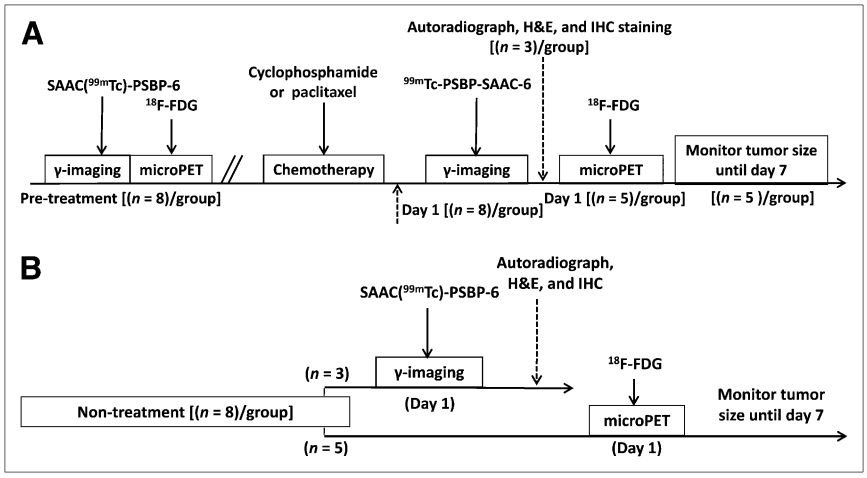

FIGURE 1. Design of study comparing γ-imaging using SAAC(^{99m}Tc)-PSBP-6 with small-animal PET using ^{18}F-FDG in tumor-bearing mice after chemotherapy: TG (A) and N-TG (B). IHC = immunohistochemical.

and eosin (H&E) staining, and immunohistochemical staining for apoptotic cells (terminal deoxynucleotidyl transferase –mediated dUTP nick end labeling [TUNEL] and anti–active caspase 3). The remaining 5 mice underwent ^{18}F-FDG small-animal PET, and these mice were then monitored for tumor growth using caliper measurements every other day for 7 d. In the N-TG, 3 mice received an intravenous injection of SAAC(^{99m}Tc)-PSBP-6 (7.4 MBq [200 μCi]/mouse) for γ-imaging on day 1. The mice were killed immediately after the imaging session, and tumor tissues were resected for autoradiography, H&E staining, and immunohistochemical staining. The remaining 5 mice in the N-TG were imaged with ^{18}F-FDG small-animal PET on day 1. The tumors were measured using calipers every other day for 7 d.

For the 10 mice that were monitored for 7 d, tumor volume was calculated using the following equation: tumor volume = 1/2 (length × width^2). Mice were euthanized by CO_2 inhalation on day 7.

γ-Imaging and Data Analysis

γ-imaging was performed at 4 h after injection of SAAC(^{99m}Tc)-PSBP-6. Fifteen-minute planar γ-images were acquired using an M-CAM camera (Siemens Medical Solutions USA) with a low-energy high-resolution collimator and ICON software (Siemens Medical Solutions USA). Image acquisition parameters were as follows: matrix, 512 × 512; zoom, 3.20; and energy peaks, 140 keV ± 15%. For imaging analysis, regions of interest were drawn covering the whole tumor, the calibration standard, and the left thigh muscle tissue. The region-of-interest counts per pixel were used to calculate tumor-to-muscle ratios. The tumor uptake of SAAC (^{99m}Tc)-PSBP-6 was expressed as a percentage of the injected dose: %ID = tumor region-of-interest counts/injection dose ×100%.

^{18}F-FDG Small-Animal PET and Data Analysis

An R4 microPET scanner (Siemens Medical Solutions) was used for the ^{18}F-FDG PET study. The system has a resolution of approximately 2 mm in each axial direction. Mice were fasted for 12 h before ^{18}F-FDG PET scans but allowed free access to water. A 20-min prone-acquisition scan was obtained 1 h after intravenous injection of 5.6–7.4 MBq (150–200 μCi) of ^{18}F-FDG. Mice were maintained under anesthesia with 1%–2% isoflurane, and a heating lamp was used to maintain body temperature during data acquisition. Small-animal PET images were reconstructed using the ordered-subsets expectation maximization algorithm with 16 subsets and 4 iterations. For imaging data analysis, irregular 3-dimensional volumes of interest (VOIs) were manually drawn around the edges of the tumor using ASIpro VM software (Siemens Medical Solutions). Separate VOIs were drawn for each scan before and after treatment. The mean activities within the VOIs were recorded. Assuming a tissue density of 1 g/mL, the radioactivity count in each VOI was converted to MBq/g/min, and the resulting value was divided by the administered dose to obtain a percentage of the injected dose per gram of tissue (%ID/g). The change in ^{18}F-FDG uptake before and after chemotherapy was calculated according to the following formula:

$$\%\Delta = (^{18}\text{F-FDG uptake on day 1} - {}^{18}\text{F-FDG uptake on day 0})/{}^{18}\text{F-FDG uptake on day 0}$$

Histopathology, Autoradiography, and Immunohistochemical Staining

Tumor tissues were resected and immediately snap-frozen with optimum-cutting-temperature compound (Sakura Finetek). The blocks were cryosectioned into 10 consecutive 5-μm slices. Two slices were stained for H&E and 4 slices for autoradiography, and the other 4 slices were stored at –80°C and used for immunohistochemical staining. For autoradiography, the slices were dried at 40°C in open air. The slices were then photographed and exposed on BAS-SR 2025 Fuji phosphorus film for 12 h, and the film was scanned using the FLA5100 Multifunctional Imaging System (Fuji Film Life Science). For immunohistochemical staining, 2 slices were stained with TUNEL (R&D Systems) according to the manufacturer's protocol. The cell nuclei were counterstained with 6-diamidino-2-phenylindole (Sigma-Aldrich). The remaining slides were stained with anti–active caspase 3 polyclonal antibodies according to the manufacturer's protocol (Promega). All slides were visualized under a Zeiss Axio Observer.Z1 fluorescence microscope (Carl Zeiss MicroImaging GmbH).

Statistical Analysis

Group variation was described as the mean ± SD. Statistical analyses were performed to compare the uptake values for SAAC (^{99m}Tc)-PSBP-6 and ^{18}F-FDG at different times (pretherapy vs. day 1 after therapy) in the TGs and N-TGs. Mean uptake values were compared using 1-way ANOVA. A P value less than or equal to 0.05 was considered statistically significant.

RESULTS

Changes of Tumor Volume

As shown in Figure 2A, for C3H/HeJ mice bearing murine B-cell 38C13 lymphoma, tumor volumes were 0.22 ± 0.07 and 0.23 ± 0.06 cm^3, respectively, in the TG and N-TG mice on day 0; no significant difference was found between the groups before treatment. A time-dependent increase in tumor volume was observed in the N-TG, whereas in the cyclophosphamide (TG, the tumor volume decreased during the same time period. Significant differences in tumor volume were found between the TG and N-TG on days 3 (P = 0.006), 5 (P = 0.004), and 7 (P = 0.005).

Similar findings were observed in the nude mice bearing B16/F10 melanoma (Fig. 2B). No significant difference was found between the TG and N-TG, with tumor volumes of 0.35 ± 0.10 and 0.31 ± 0.04 cm^3, respectively, on day 0. On day 3, tumor volumes were 0.11 ± 0.04 and 0.94 ± 0.37 cm^3 for the PG-TXL TG and N-TG, respectively (P = 0.007). Tumor volumes continued to increase for mice in the N-TG and decrease for mice in the TG on days 5 and 7.

Comparison of ^{18}F-FDG and SAAC(^{99m}Tc)-PSBP-6 Uptake in 38C13 Lymphoma

Figure 3A shows small-animal PET images of 38C13 tumors with ^{18}F-FDG before and after cyclophosphamide treatment. Figure 3B shows γ-images of 38C13 tumors with SAAC(^{99m}Tc)-PSBP-6 before and after cyclophosphamide treatment. The changes in ^{18}F-FDG and SAAC(^{99m}Tc)-PSBP-6 uptake values before and after treatment are summarized in Supplemental Figures 2A and 2B, respectively. The mean tumor uptake value of ^{18}F-FDG decreased significantly from 2.23 ± 0.91 %ID/g before treatment to 0.72 ± 0.49 %ID/g on day 1 after treatment (P = 0.005). In contrast, the tumor uptake of the apoptosis marker

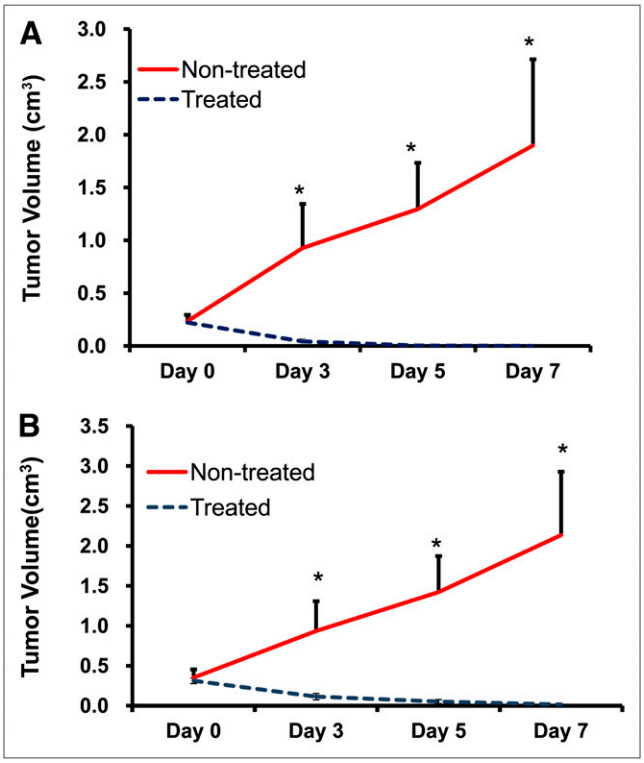

FIGURE 2. Tumor growth delays after chemotherapy. (A) C3H/HeJ mice bearing murine 38C13 B-cell lymphoma were treated with intraperitoneal injection of cyclophosphamide at dose of 100 mg/kg. (B) Nude mice bearing B16/F10 melanoma were treated with intravenous injection of PG-TXL at equivalent paclitaxel dose of 80 mg/kg. *$P < 0.01$. IHC = immunohistochemical.

SAAC(^{99m}Tc)-PSBP-6 increased significantly, from 0.27 ± 0.05 %ID before treatment to 0.65 ± 0.06 %ID on day 1 after treatment ($P = 0.0002$).

Figures 4A and 4B show representative autoradiographs and H&E-, TUNEL-, and active caspase 3–stained slides of 38C13 tumors from mice in the N-TGs and TGs, respectively. Compared with untreated tumors, treatment with cyclophosphamide caused cell shrinkage, chromatin condensation, and extensive apoptotic response.

Comparison of ^{18}F-FDG and SAAC(^{99m}Tc)-PSBP-6 Uptake in B16/F10 Melanoma

Figure 5A shows small-animal PET images of B16/F10 tumors with ^{18}F-FDG before and after PG-TXL treatment. Figure 5B shows γ-images of B16/F10 tumors with SAAC(^{99m}Tc)-PSBP-6 before and after PG-TXL treatment. The changes of ^{18}F-FDG and SAAC(^{99m}Tc)-PSBP-6 uptake values before and after treatment are summarized in Supplemental Figure 3A and Figure 3B, respectively. The mean tumor uptake value of ^{18}F-FDG decreased significantly from 3.73 ± 0.81 %ID/g before treatment to 1.44 ± 0.46 %ID/g on day 1 after treatment ($P = 0.001$). On the other hand, the tumor uptake of SAAC(^{99m}Tc)-PSBP-6 increased significantly from 1.61 ± 0.33 %ID before treatment to 4.06 ± 0.55 %ID on day 1 after treatment ($P = 0.002$).

Supplemental Figures 4A and 4B show representative autoradiographs and H&E-, TUNEL-, and active caspase 3–stained slides of B16/F10 tumors from mice in the N-TGs and TGs, respectively. Similar to what was observed in the 38C13 tumors treated with cyclophosphamide, treatment of B16/F10 tumors with PG-TXL induced extensive apoptosis on day 1 after treatment.

Additional biodistribution data of SAAC(^{99m}Tc)-PSBP-6 at 4 h after injection in 38C13 and B16/F10 tumor models with and without treatments are shown in Supplemental Figures 5 and 6, respectively. Chemotherapy resulted in significantly higher tumor uptake of SAAC(^{99m}Tc)-PSBP-6 in both 38C13 and B16/F10 tumor models ($P = 0.0007$ and 0.0005, respectively). Interestingly, treatment with cyclophosphamide also caused significantly higher uptake of SAAC(^{99m}Tc)-PSBP-6 in the heart ($P = 0.0055$), suggesting that the drug may have caused apoptosis of cells of the myocardium. Cyclophosphamide is known to induce acute cardiotoxicity (*27*). Further studies are needed to confirm the role of SAAC (^{99m}Tc)-PSBP-6 in imaging cardiotoxicity.

DISCUSSION

In this study, we found that γ-imaging with the apoptosis-avid agent SAAC(^{99m}Tc)-PSBP-6 revealed an increased

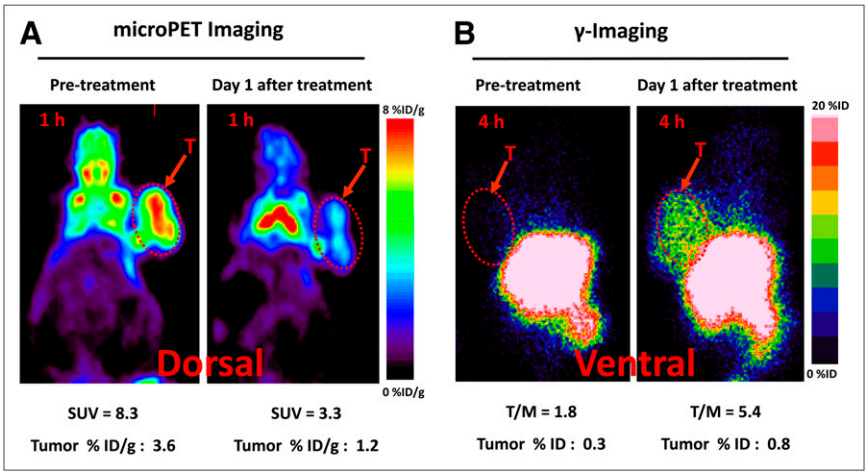

FIGURE 3. Representative images of 38C13 tumor–bearing mice before and 1 d after treatment with cyclophosphamide (intraperitoneal, 100 mg/kg). (A) Small-animal PET images acquired 1 h after ^{18}F-FDG injection. (B) γ-images obtained 4 h after SAAC(^{99m}Tc)-PSBP-6 injection. SUV = standardized uptake value; T = tumors; T/M = tumor-to-muscle ratio.

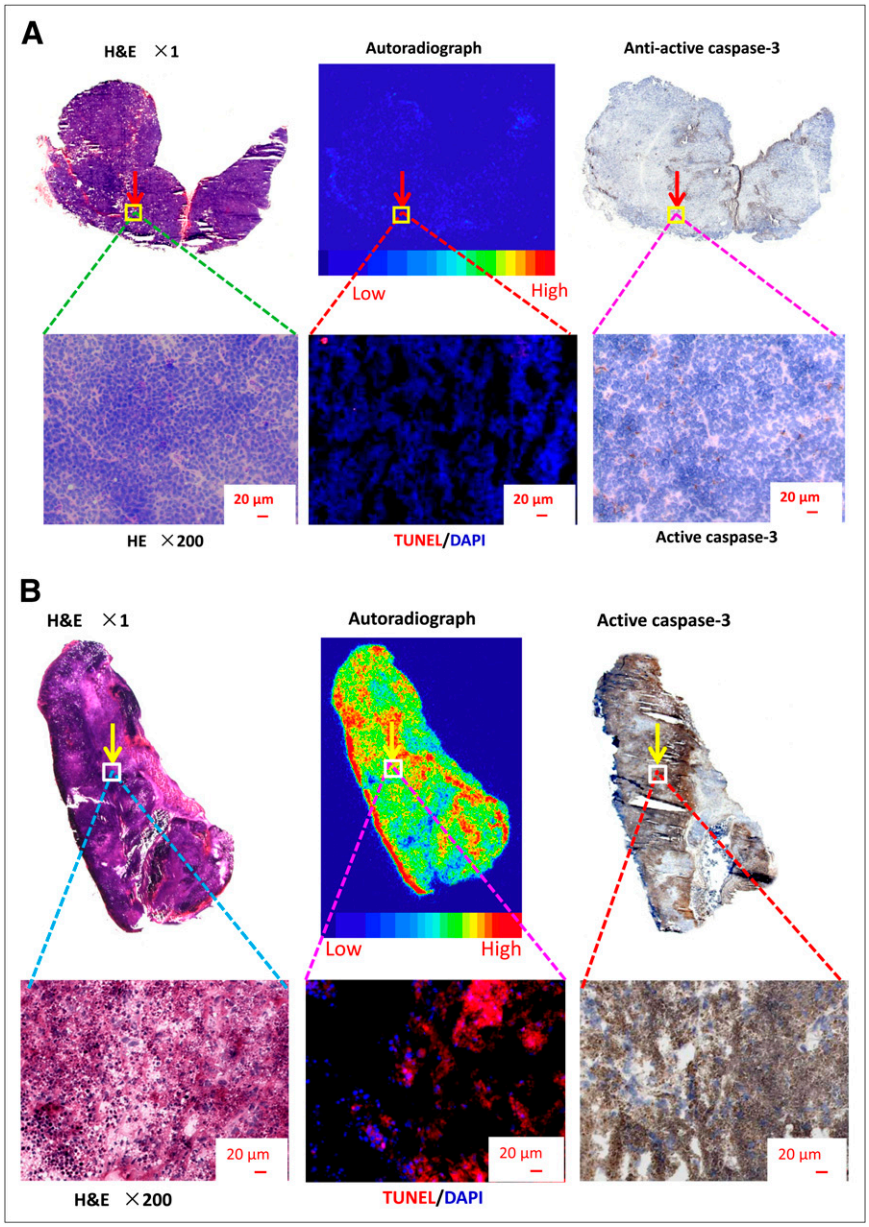

FIGURE 4. Representative autoradiographs and photographs of H&E-, TUNEL-, and active caspase 3–stained slides of 38C13 tumors from nontreated mouse (A) and cyclophosphamide-treated mouse (B). Tumors were removed at 4 h after intravenous injection of SAAC(^{99m}Tc)-PSBP-6. Red in fluorescent microphotographs shows TUNEL-positive apoptotic cells; blue represents 6-diamidino-2-phenylindole (DAPI)–stained cells.

uptake of the agent in tumors after 2 different chemotherapy regimens in 2 different tumor models. As expected, the same treatments resulted in a decreased uptake of ^{18}F-FDG. The uptake of SAAC(^{99m}Tc)-PSBP-6 negatively correlated with ^{18}F-FDG ($r = -0.79$, $P < 0.05$). Moreover, the treatments induced extensive apoptosis on day 1 after therapy and caused tumor regression over a period of 7 d. Thus, our data support the use of SAAC(^{99m}Tc)-PSBP-6 as a potential imaging agent for assessing early apoptotic response after anticancer therapy.

Apoptosis plays an essential role in various diseases; noninvasive detection of apoptosis may serve as a useful tool in clinical practice. In anticancer therapy, successful treatments often result in apoptosis of cancer cells at an early stage (*28,29*); thus, imaging of apoptosis is a logical approach to the assessment of early response to anticancer therapy. Phosphatidylserine is a membrane-associated intracellular phospholipid that is invariably expressed on the external cell membrane surface early in the apoptotic cascade. Various agents directed at phosphatidylserine, most notably annexin V, have been investigated as potential apoptosis-imaging agents (*15–18,30–34*). However, annexin V is rapidly cleared from the blood, and because of its relatively high molecular weight, its penetration into the tumor matrix is thought to be limited. Therefore, there is room for improving the sensitivity of apoptosis detection with the next generation of phosphatidylserine-avid imaging agents.

We have taken 2 approaches in an effort to improve the sensitivity of apoptosis detection. The first approach was to modulate the pharmacokinetics of annexin V in such a way as to increase its blood half-life, thereby increasing the chances of capturing apoptotic cells. The validity of this

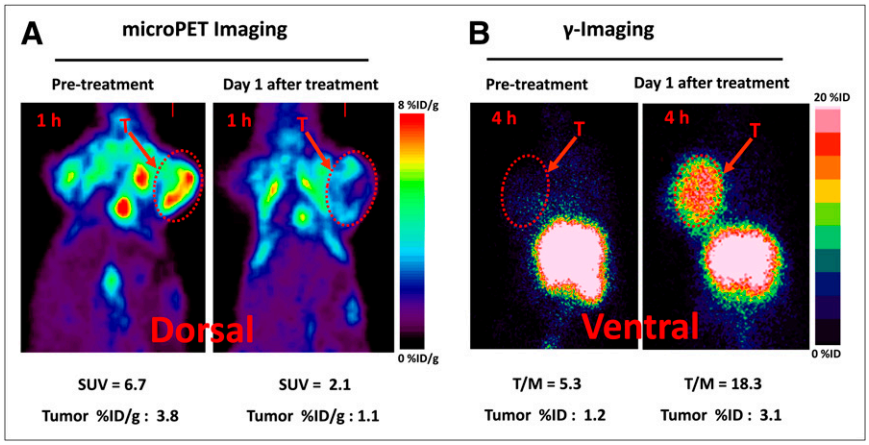

FIGURE 5. Representative images of B16/F10 tumor–bearing mice before and 1 d after treatment with PG-TXL (intravenous, equivalent TXL dose = 80 mg/kg). (A) Small-animal PET images acquired 1 h after ^{18}F-FDG injection. (B) γ-images obtained 4 h after SAAC(^{99m}Tc)-PSBP-6 injection. SUV = standardized uptake value; T = tumors; T/M = tumor-to-muscle ratio.

approach has been demonstrated recently by conjugating annexin V to multifunctional long-circulating polymeric micelles (*18*). The second approach was to develop small-molecular-weight imaging agents that can bind to phosphatidylserine with affinity similar to or better than that of annexin V. The premise is that small-molecular-weight compounds may have better diffusibility in the tumor mass than large-molecular-weight compounds because the rate of diffusion is inversely proportional to the size of the molecule.

Through a structure–activity study and targeted library-based screening, we identified the 14-mer peptide PSBP-6 that, when conjugated with a single amino acid metal chelator at the N terminus of the peptide, displayed a phosphatidylserine-binding affinity of approximately 26 nM (*25*), making it a suitable apoptosis-imaging agent. SAAC(^{99m}Tc)-PSBP-6 has a much smaller molecular weight (2,045 Da) than annexin V (35,800 Da). In addition, ^{99m}Tc has an energy level of 140 keV and a half-life of 6 h, making it an ideal radionuclide for γ-camera and SPECT imaging.

B16/F10 melanoma and 38C13 lymphoma have different biologic characteristics. Higher tumor uptake is noted in both treated and untreated B16/F10 melanoma than in 38C13 lymphoma models. We found that the tumor volume doubling time is much shorter for B16/F10 than for 38C13 tumors. Faster growth may result in a higher baseline level of apoptotic cells. Moreover, different tumor types have different sensitivities to different chemotherapeutic agents. The sensitivity of tumor cells to chemotherapy drugs may directly influence the number of apoptotic cells after treatment. In our study, B16/F10 tumor models had a higher uptake of SAAC(^{99m}Tc)-PSBP-6 probe after the treatment than did 38C13, suggesting that B16/F10 tumor cells responded to taxane treatment extensively and rapidly. On the other hand, 38C13 tumor cells responded to cyclophosphamide treatment with a relatively low number of apoptosis cells on day 1 after chemotherapy. Future studies are needed to quantitatively correlate tumor uptake of SAAC(^{99m}Tc)-PSBP-6 to percentage of apoptosis before and after therapy.

Similar to annexin V–based imaging agents, SAAC (^{99m}Tc)-PSBP-6 may not specifically bind to apoptotic cells because cells undergoing necrosis also have numerous phosphatidylserine molecules accessible to phosphatidylserine-binding molecules. Another limitation of SAAC (^{99m}Tc)-PSBP-6 is the high background signal in the abdominal area preventing the use of this agent for imaging lesions in the liver and gastrointestinal tract.

CONCLUSION

γ-imaging with SAAC(^{99m}Tc)-PSBP-6 could be used to assess early response to chemotherapy-induced apoptosis. Further studies in various preclinical models of apoptosis are needed to further investigate the sensitivity and specificity of this agent.

DISCLOSURE

The costs of publication of this article were defrayed in part by the payment of page charges. Therefore, and solely to indicate this fact, this article is hereby marked "advertisement" in accordance with 18 USC Section 1734. This work was funded in part by the John S. Dunn Foundation, the National Natural Science Foundation of China (grants 30830038, 81071180, and 81101073), and the Shanghai Pujiang Program. No other potential conflict of interest relevant to this article was reported.

ACKNOWLEDGMENT

We thank Dawn Chalaire, Department of Scientific Publications Anderson Cancer Center, for editing the manuscript.

REFERENCES

1. Wahl RL, Jacene H, Kasamon Y, Lodge MA. From RECIST to PERCIST: evolving considerations for PET response criteria in solid tumors. *J Nucl Med.* 2009;50(suppl 1):122S–150S.
2. Gambhir SS. Molecular imaging of cancer with positron emission tomography. *Nat Rev Cancer.* 2002;2:683–693.
3. Ott K, Weber WA, Lordick F, et al. Metabolic imaging predicts response, survival, and recurrence in adenocarcinomas of the esophagogastric junction. *J Clin Oncol.* 2006;24:4692–4698.
4. Weissleder R. Molecular imaging in cancer. *Science.* 2006;312:1168–1171.
5. Bleeker-Rovers CP, Vos FJ, van der Graaf WT, Oyen WJ. Nuclear medicine imaging of infection in cancer patients (with emphasis on FDG-PET). *Oncologist.* 2011;16:980–991.

6. Ben-Haim S, Ell P. ^{18}F-FDG PET and PET/CT in the evaluation of cancer treatment response. *J Nucl Med.* 2009;50:88–99.
7. Alberini JL, Lerebours F, Wartski M, et al. ^{18}F-fluorodeoxyglucose positron emission tomography/computed tomography (FDG-PET/CT) imaging in the staging and prognosis of inflammatory breast cancer. *Cancer.* 2009;115:5038–5047.
8. Shah C, Miller TW, Wyatt SK, et al. Imaging biomarkers predict response to anti-HER2 (ErbB2) therapy in preclinical models of breast cancer. *Clin Cancer Res.* 2009;15:4712–4721.
9. Thompson CB. Apoptosis in the pathogenesis and treatment of disease. *Science.* 1995;267:1456–1462.
10. Abend M. Reasons to reconsider the significance of apoptosis for cancer therapy. *Int J Radiat Biol.* 2003;79:927–941.
11. Kerr JF, Winterford CM, Harmon BV. Apoptosis: its significance in cancer and cancer therapy. *Cancer.* 1994;73:2013–2026.
12. Schimmer AD, Welsh K, Pinilla C, et al. Small-molecule antagonists of apoptosis suppressor XIAP exhibit broad antitumor activity. *Cancer Cell.* 2004;5:25–35.
13. Fulda S, Susin SA, Kroemer G, Debatin KM. Molecular ordering of apoptosis induced by anticancer drugs in neuroblastoma cells. *Cancer Res.* 1998;58:4453–4460.
14. De Saint-Hubert M, Bauwens M, Verbruggen A, Mottaghy FM. Apoptosis imaging to monitor cancer therapy: the road to fast treatment evaluation? *Curr Pharm Biotechnol.* 2012;13:571–583.
15. Blankenberg FG, Katsikis PD, Tait JF, et al. In vivo detection and imaging of phosphatidylserine expression during programmed cell death. *Proc Natl Acad Sci USA.* 1998;95:6349–6354.
16. Yagle KJ, Eary JF, Tait JF, et al. Evaluation of ^{18}F-annexin V as a PET imaging agent in an animal model of apoptosis. *J Nucl Med.* 2005;46:658–666.
17. Tait JF, Smith C, Blankenberg FG. Structural requirements for in vivo detection of cell death with ^{99m}Tc-annexin V. *J Nucl Med.* 2005;46:807–815.
18. Zhang R, Lu W, Wen X, et al. Annexin A5-conjugated polymeric micelles for dual SPECT and optical detection of apoptosis. *J Nucl Med.* 2011;52:958–964.
19. Zhu X, Li Z, Zhao M. Imaging acute cardiac cell death: temporal and spatial distribution of ^{99m}Tc-labeled C2A in the area at risk after myocardial ischemia and reperfusion. *J Nucl Med.* 2007;48:1031–1036.
20. Wang F, Fang W, Zhao M, et al. Imaging paclitaxel (chemotherapy)-induced tumor apoptosis with ^{99m}Tc C2A, a domain of synaptotagmin I: a preliminary study. *Nucl Med Biol.* 2008;35:359–364.
21. Chen DL, Zhou D, Chu W, et al. Comparison of radiolabeled isatin analogs for imaging apoptosis with positron emission tomography. *Nucl Med Biol.* 2009;36:651–658.
22. Smith G, Glaser M, Perumal M, et al. Design, synthesis, and biological characterization of a caspase 3/7 selective isatin labeled with 2-[^{18}F]fluoroethylazide. *J Med Chem.* 2008;51:8057–8067.
23. Reshef A, Shirvan A, Akselrod-Ballin A, Wall A, Ziv I. Small-molecule biomarkers for clinical PET imaging of apoptosis. *J Nucl Med.* 2010;51:837–840.
24. Lahorte CM, Vanderheyden JL, Steinmetz N, Van de Wiele C, Dierckx RA, Slegers G. Apoptosis-detecting radioligands: current state of the art and future perspectives. *Eur J Nucl Med Mol Imaging.* 2004;31:887–919.
25. Xiong C, Brewer K, Song S, et al. Peptide-based imaging agents targeting phosphatidylserine for the detection of apoptosis. *J Med Chem.* 2011;54:1825–1835.
26. Li C, Yu DF, Newman RA, et al. Complete regression of well-established tumors using a novel water-soluble poly(L-glutamic acid)-paclitaxel conjugate. *Cancer Res.* 1998;58:2404–2409.
27. Gharib MI, Burnett AK. Chemotherapy-induced cardiotoxicity: current practice and prospects of prophylaxis. *Eur J Heart Fail.* 2002;4:235–242.
28. Schmitt CA, Lowe SW. Apoptosis is critical for drug response in vivo. *Drug Resist Updat.* 2001;4:132–134.
29. Tolomeo M, Simoni D. Drug resistance and apoptosis in cancer treatment: development of new apoptosis-inducing agents active in drug resistant malignancies. *Curr Med Chem Anticancer Agents.* 2002;2:387–401.
30. Swairjo MA, Seaton BA. Annexin structure and membrane interactions: a molecular perspective. *Annu Rev Biophys Biomol Struct.* 1994;23:193–213.
31. Gerke V, Creutz CE, Moss SE. Annexins: linking Ca2+ signalling to membrane dynamics. *Nat Rev Mol Cell Biol.* 2005;6:449–461.
32. Skaane P. Molecular imaging: a potential new tool for early detection and monitoring of targeted breast cancer therapy. *Acta Radiol.* 2009;50:1092–1093.
33. Kenis H, Hofstra L, Reutelingsperger CP. Annexin A5: shifting from a diagnostic towards a therapeutic realm. *Cell Mol Life Sci.* 2007;64:2859–2862.
34. Takei T, Kuge Y, Zhao S, et al. Enhanced apoptotic reaction correlates with suppressed tumor glucose utilization after cytotoxic chemotherapy: use of ^{99m}Tc-Annexin V, ^{18}F-FDG, and histologic evaluation. *J Nucl Med.* 2005;46:794–799.